

# Fe<sup>3+</sup> and Fe<sup>2+</sup> center in GaN

E. Malguth,\* A. Hoffmann, and W. Gehlhoff

*Institut für Festkörperphysik, Technische Universität Berlin, Hardenbergstraße 36, 10623 Berlin, Germany*

O. Gelhausen and M. R. Phillips

*Microstructural Analysis Unit, University of Technology, Sydney, Broadway, NSW 2007 Australia*

X. Xu<sup>†</sup>

*Cree, Inc., 4600 Silicon Drive, Durham, NC 27703, USA*

(Dated: August 4, 2006)

This work provides a consistent picture of the structural, optical and electronic properties of Fe doped GaN. A set of high-quality GaN crystals doped with Fe at concentrations ranging from  $5 \times 10^{17} \text{ cm}^{-3}$  to  $2 \times 10^{20} \text{ cm}^{-3}$  is systematically investigated by means of electron paramagnetic resonance and various optical techniques. Fe<sup>3+</sup> is shown to be a stable charge state at concentrations from  $1 \times 10^{18} \text{ cm}^{-3}$ . The fine structure of its mid-gap states is successfully established including an effective-mass-like state consisting of a hole bound to Fe<sup>2+</sup> with a binding energy of  $50 \pm 10 \text{ meV}$ . A major excitation mechanism of the Fe<sup>3+</sup> (<sup>4</sup>T<sub>1</sub>—<sup>6</sup>A<sub>1</sub>) luminescence is identified to be the capture of free holes by Fe<sup>2+</sup> centers. The holes are generated in a two step process via the intrinsic defects involved in the yellow luminescence. The Fe<sup>3+/2+</sup> charge transfer level is found  $2.863 \pm 0.005 \text{ eV}$  above the valence band, suggesting that the internal reference rule does not hold for the prediction of band off-sets of heterojunctions between GaN and other III-V materials. The Fe<sup>2+</sup> (<sup>5</sup>E—<sup>5</sup>T<sub>2</sub>) transition is observed around 390 meV at any studied Fe concentration by means of Fourier transform infrared spectroscopy. Charge transfer processes and the effective-mass-like state involving both Fe<sup>2+</sup> states are observed. At Fe concentrations from  $1 \times 10^{19} \text{ cm}^{-3}$ , additional lines occur in EPR and PL spectra which are attributed to defect complexes involving Fe<sup>3+</sup>. With increasing Fe concentration, the Fermi level is shown to move from near the conduction band to the Fe<sup>3+/2+</sup> charge transfer level, where it stays pinned for concentrations from  $1 \times 10^{19} \text{ cm}^{-3}$ . Contrary to cubic II-VI and III-V materials, both electronic states are effected by only a weak Jahn-Teller interaction.

PACS numbers: 12345

## I. INTRODUCTION

Acting as a deep acceptor, iron is currently introduced into GaN to compensate inherent n-type conductivity and to produce semi-insulating substrate material necessary for the production of high performance GaN/AlGaIn high electron mobility transistors (HEMTs).<sup>1-3</sup> Moreover, Fe doped GaN is widely considered to be a potential material to realize future spintronic applications. However, the impact of Fe on the optical, electrical and magnetic properties of GaN is not well understood, and hence they cannot be sufficiently controlled at present. In particular for spintronic applications, a detailed knowledge of the occurring charge states and their respective electronic structure is crucial to model carrier mediated ferromagnetism.<sup>4,5</sup> Of great importance is a knowledge of the exact position of the Fe<sup>3+/2+</sup> acceptor level within the band gap because it is used to predict band off-sets in hetero structures on the basis of the internal reference rule.<sup>6,7</sup> Furthermore, the behavior of d<sup>5</sup> and d<sup>6</sup> systems in a trigonal crystal field of c<sub>3v</sub> symmetry is of general physical interest for aspects of group and crystal field theory.

In GaN with a wurtzite lattice type, the Ga-site has a tetrahedral symmetry that is tetragonally distorted along the c-axis resulting in c<sub>3v</sub> symmetry. To a good approximation, the crystal field can be considered to be equiv-

alent to the perfect tetrahedral T<sub>d</sub> symmetry present in cubic crystals (zinc blende). The impact of the ligand field in form of a Stark effect causes the d<sup>5</sup> configuration of Fe<sup>3+</sup> on Ga site to split into the ground state <sup>6</sup>A<sub>1</sub>(S) and the excited states <sup>4</sup>T<sub>1</sub>(G), <sup>4</sup>T<sub>2</sub>(G) and <sup>4</sup>E(G).<sup>8</sup> The spin-forbidden (<sup>4</sup>T<sub>1</sub>(G)—<sup>6</sup>A<sub>1</sub>(S)) transition is observed as an IR luminescence at 1.299 eV with a lifetime of 8 ms and has been unequivocally assigned by Zeeman experiments.<sup>9-11</sup> Spin and parity selection rules are relaxed under the influence of the c<sub>3v</sub> crystal field, and lattice strain can shift the emission line by  $\sim 1 \text{ meV}$ .<sup>10</sup> Three further lines are reported to appear at higher temperatures reflecting the fine structure of the <sup>4</sup>T<sub>1</sub>(G) state.<sup>10,11</sup> Heitz et al. found the higher excited states <sup>4</sup>T<sub>2</sub>(G) and <sup>4</sup>E(G) at 2.01 and 2.731 eV above the ground state, respectively, and also identified an exciton bound to the Fe center constituting a shallow acceptor state (Fe<sup>3+</sup>,e,h) at 2.888 eV above the ground state.<sup>8</sup> Based on the established position of the Fe<sup>3+/2+</sup> charge transfer (CT) level at 3.17 eV above the valence band (VB) the following conclusions were drawn by these workers: (i) The binding energy of the bound state is 280 meV, (ii) the Fe<sup>2+</sup> (<sup>5</sup>T<sub>2</sub>) state is degenerated with the conduction band (CB), and (iii) the internal reference rule fails for GaN in conjunction with other III-V materials, including nitrides.<sup>6-8</sup>

The <sup>5</sup>D ground state of the Fe<sup>2+</sup> center of d<sup>6</sup> configura-

TABLE I: Resistivity of Fe-doped GaN samples measured by ATMI at room temperature.

Fe conc. ( $\text{cm}^{-3}$ )	Resistivity ( $\Omega \text{ cm}$ )
$5 \times 10^{17}$	200
$1 \times 10^{18}$	$1 \times 10^8$
$1 \times 10^{19}$	$3 \times 10^8$
$2 \times 10^{20}$	900

tion splits into the states  ${}^5\text{E}$  and  ${}^5\text{T}_2$  under the influence of the ligand field. While the transition between these two has been reported for cubic III-V materials, it is believed to be absent in GaN.<sup>12</sup>

In this work, we present a systematic study of the physical properties of Fe doped GaN with a particular focus on the electronic structure of the detected 3+ and 2+ charge states. The fine structure of all observed  $\text{Fe}^{3+}$  states is established, while a forthcoming paper is dedicated to the fine structure of the  $\text{Fe}^{2+}$  states  ${}^5\text{E}$  and  ${}^5\text{T}_2$ .<sup>13</sup> High quality samples have facilitated precise determination of Fe related energy states in GaN:Fe. Major corrections of the previously reported bound state and the energy position of the  $\text{Fe}^{3+/2+}$  CT level are also made. Finally, we report the presence of the  $\text{Fe}^{2+}({}^5\text{E} \rightarrow {}^5\text{T}_2)$  transition in GaN. A comprehensive picture of the electronic properties of Fe centers in GaN is developed by studying GaN with varying Fe concentration using a broad array of spectroscopies, including electron paramagnetic resonance (EPR), photo luminescence (PL), transmission spectroscopy, PL excitation (PLE) and Fourier transform infra red spectroscopy (FTIR).

## II. EXPERIMENTAL DETAILS

A set of Fe doped GaN samples grown by ATMI using HVPE on sapphire substrate were investigated in this work. The epilayers had a wurzite crystal structure with their  $c$ -axis aligned to the growth direction. Iron was incorporated during the growth process at concentrations ranging from  $5 \times 10^{17} \text{ cm}^{-3}$  to  $2 \times 10^{20} \text{ cm}^{-3}$  as determined by secondary ion mass spectroscopy (SIMS). The substrate was removed resulting in  $\sim 400 \mu\text{m}$  thick free standing samples which were cut into pieces of approximately  $(2 \times 2)$  mm. These samples facilitated optical experiments with the light traveling perpendicular to the  $c$ -axis providing enhanced absorption and polarized spectroscopy measurements. The samples' conductivities are presented in Table I.

For PL experiments and transmission spectroscopy in the ultraviolet to visible (UV-VIS) spectral region, the samples were kept in liquid helium at a temperature of 1.8 K with the  $c$ -axis perpendicular to the optical path. PL was excited by the 2.412 eV line of an Ar ion laser. The emitted light was passed through a polarizer and

dispersed by a 1 m Spex double monochromator and detected by a nitrogen cooled Ge-detector. For UV-VIS transmission spectroscopy, depending on the spectral region, a xenon lamp or halogen-tungsten lamp in combination with a polarizer served as light sources. The transmitted light was dispersed by a 1m Jarrel-Ash monochromator and detected by a photomultiplier based on bialkali, GaAs or Ge. Fourier transform infrared (FTIR) transmission measurements were carried out using the IFS 66v spectrometer from Bruker with a globar, KBr beam-splitter and HgCdTe based detector. The samples were cooled to 50 K by a liquid helium contact cryostat with KBr windows. In PLE experiments, the samples were cooled down to 7 K. A halogen lamp in combination with a 275 mm double monochromator served as tunable light source providing a resolution of 5 meV. A 300 mm double monochromator with the same resolution was used in detection. The EPR measurements were carried out using a Bruker ESP 300E spectrometer operating at the X-band ( $\cong 9.5 \text{ GHz}$ ). A temperature of 4 K was achieved with an Oxford Instruments continuous flow cryostat.

## III. RESULTS AND DISCUSSION

In this section, first, the influence of Fe doping on the crystalline quality and the electrical properties of GaN is discussed. Second, high-resolution optical studies by PL, PLE and transmission spectroscopy were performed to understand the nature of the  $\text{Fe}^{3+}$  and the  $\text{Fe}^{2+}$  centers in GaN.

### A. Electron Paramagnetic Resonance

The structural quality of the Fe doped GaN samples was analyzed by electron paramagnetic resonance (EPR) measurements. In Fig. 1, an EPR spectrum (B|| $c$ -axis) for a Fe doped GaN sample with a Fe concentration of  $1 \times 10^{19} \text{ cm}^{-3}$  is depicted. It displays five sharp fine structure transitions that are typical for an  $S = \frac{5}{2}$  ion in axial ( $c_{3v}$ ) symmetry and are unambiguously assigned to the  $d^5$  configuration of the  $\text{Fe}^{3+}$  center on Ga site. The lines belong to the transitions  $(-\frac{1}{2} \longleftrightarrow +\frac{1}{2})$ ,  $(\pm\frac{3}{2} \longleftrightarrow \pm\frac{1}{2})$  and  $(\pm\frac{5}{2} \longleftrightarrow \pm\frac{3}{2})$  with  $\Delta M = \pm 1$  (in the order of decreasing intensity). Compared with previous studies,<sup>9</sup> the samples investigated in this work are of much higher crystal quality and do not exhibit a random strain broadening. This fact is supported by the sharpness of the outer line pairs of fine structure transitions  $(\pm\frac{5}{2} \longleftrightarrow \pm\frac{3}{2})$ , which indicates that the Fe centers are incorporated relatively strain free. A similar high quality EPR spectrum is observed at 300 K as well. Due to the high Debye temperature of GaN (600 K), spin-lattice relaxation does not result in excessive EPR line broadening at room temperature.<sup>14</sup> In connection with additional EPR measurements in the Q-band (34 GHz), the smaller

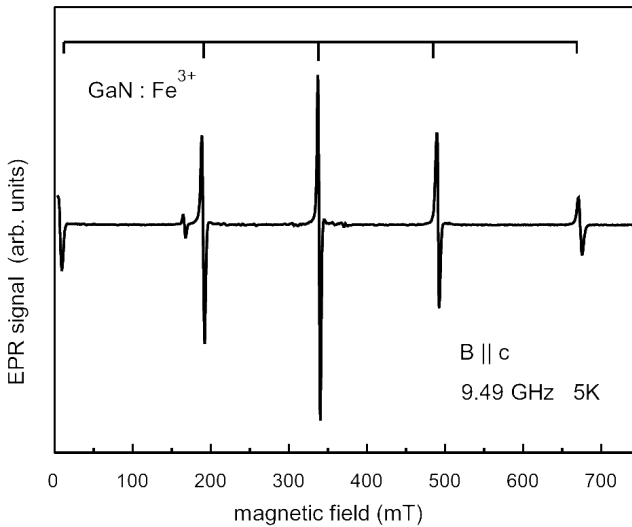


FIG. 1: X-band EPR spectrum of Fe doped GaN with a Fe concentration of  $1 \times 10^{19} \text{ cm}^{-3}$  at 4 K for  $B \parallel c$ -axis. The line positions of the five allowed fine-structure transitions ( $\Delta M = \pm 1$ ) are indicated

line widths seen in Fig. 1 allow to determine the spin Hamiltonian parameters more accurately than in previous works.<sup>15</sup>

Other Fe charge states than  $\text{Fe}^{3+}$  were not detected by EPR experiments.

## B. Photo Luminescence

Near infrared PL spectra of Fe doped GaN are shown Fig. 2 for various Fe concentrations. The typical  $\text{Fe}^{3+}({}^4\text{T}_1(\text{G}) \rightarrow {}^6\text{A}_1(\text{S}))$  transition with a vibrational sideband is observed at any investigated Fe concentration. The position and the full width at half maximum (FWHM) of the zero phonon line (ZPL) as a function of the Fe concentration are displayed in Fig. 5 (a) and (b), respectively. The observed FWHM which is as low as  $120 \mu\text{eV}$  confirms the good crystal quality and strain free incorporation of iron as suggested by EPR measurements. The increasing FWHM with rising Fe concentration is probably due to the modified crystal field caused by the substitution of Ga by Fe ions which is only felt by neighboring Fe centers at high Fe densities. The concentration of  $\text{Fe}^{3+}$  centers is expected to scale with the overall iron content due to the shift of the Fermi level discussed above. However, the intensity of the  $\text{Fe}^{3+}$  related luminescence observed herein is independent on the Fe concentration. Incomplete excitation of the  $\text{Fe}^{3+}$  due to an insufficient laser intensity is quite unlikely to account for this observation because of the long life time (8 ms) of the spin forbidden transition<sup>11</sup>. Consequently, an extra-center excitation process, which is still to be identified, must be the bottleneck.

A closer investigation of the ZPL of the sample with

a Fe concentration of  $1 \times 10^{19} \text{ cm}^{-3}$  at an increased excitation intensity is presented in Fig. 3. Additional lines on the high-energy side can be observed 1.10, 1.72, 2.42, and 3.65 meV above the the ZPL at 1.299 eV. The latter three lines have been observed before in experiments at 10 K.<sup>10,11</sup>

The  ${}^6\text{A}_1(\text{S})$  state of  $\text{Fe}^{3+}$  splits, due to the spin-orbit-coupling, into states of  $\Gamma_7$  and  $\Gamma_8$  symmetry separated by only  $9 \mu\text{eV}$  which is negligible compared with the linewidth. Therefore, the additional peaks represent transitions starting at excited  ${}^4\text{T}_1(\text{G})$  sub-levels. The exact fine structure of  ${}^4\text{T}_1(\text{G})$  state is the result of spin-orbit coupling, the Jahn-Teller effect as well as the axial distortion of the trigonal crystal field in  $c_{3v}$  symmetry of the wurtzite lattice structure. Spin-orbit interaction causes a splitting into four states of  $\Gamma_6$ ,  $\Gamma_8$ ,  $\Gamma_7$  and  $\Gamma_8$  symmetry. In cubic II-VI and III-V crystals a strong Jahn-Teller effect involving E-type phonon modes quenches the orbital momentum reducing the fourfold splitting to a doublet with a splitting of about 1 meV.<sup>16-18</sup> However, the fivefold splitting of about 4 meV observed in Fig. 3 indicates only a weak or intermediate Jahn-Teller interaction. The lower defect symmetry in wurtzite structure stabilizes the  $\text{Fe}^{3+}$  center against the Jahn-Teller coupling as has been established for the  ${}^4\text{T}_1(\text{G})$  state in ZnO.<sup>19</sup> Moreover, a splitting of at least one spin-orbit state in  $c_{3v}$  symmetry needs to be taken into account to understand the fivefold splitting. It should be noted that the first peak above the ZPL (1.1 meV) is the smallest. This observation suggests that a selection rule is softened by the  $c_{3v}$  crystal field causing the second most populated state to exhibit the lowest intensity.

The observed polarization of each emission line in Fig. 3 allows us to tentatively assign them to  ${}^4\text{T}_1(\text{G})$  sub-states and, consequently, to derive the fine structure of the  ${}^4\text{T}_1(\text{G})$  state in  $c_{3v}$  crystal field symmetry. The result is depicted in Fig. 4. As mentioned above, spin-orbit coupling results in four states of  $\Gamma_6$ ,  $\Gamma_8$ ,  $\Gamma_7$  and  $\Gamma_8$  symmetry (see brackets in Fig. 4) which under the the impact of axial distortion ( $c_{3v}$  symmetry) of the crystal field transform as follows:

$$\begin{aligned} \Gamma_6 &\longrightarrow \Gamma_4 \\ \Gamma_7 &\longrightarrow \Gamma_4 \\ \Gamma_8 &\longrightarrow \Gamma_4, \Gamma_5, \Gamma_6 \end{aligned}$$

removing the degeneracy of the  $\Gamma_8$  states. Only the splitting of the lower  $\Gamma_8$  state is resolved. In comparison to the  $\text{Fe}^{3+}({}^4\text{T}_1(\text{G}))$  state in ZnO, the energetic positions of the top spin-orbit states ( $\Gamma_7$  and  $\Gamma_8$ ) are swapped<sup>19</sup> because the trigonal crystal field is stretched in ZnO, while it is compressed in GaN. The observed 4 meV splitting of the  ${}^4\text{T}_1(\text{G})$  state is consistent with the same state in ZnO.<sup>19</sup>

The sideband of the  $\text{Fe}^{3+}({}^4\text{T}_1(\text{G}) \rightarrow {}^6\text{A}_1(\text{S}))$  luminescence, which is displayed in Fig. 2(a1)-(d1), is a superposition of vibrational replica of the ZPL at 1.299 eV and additional sharp lines (FWHM=400  $\mu\text{eV}$ ), which are marked by dashed lines. The latter are only present

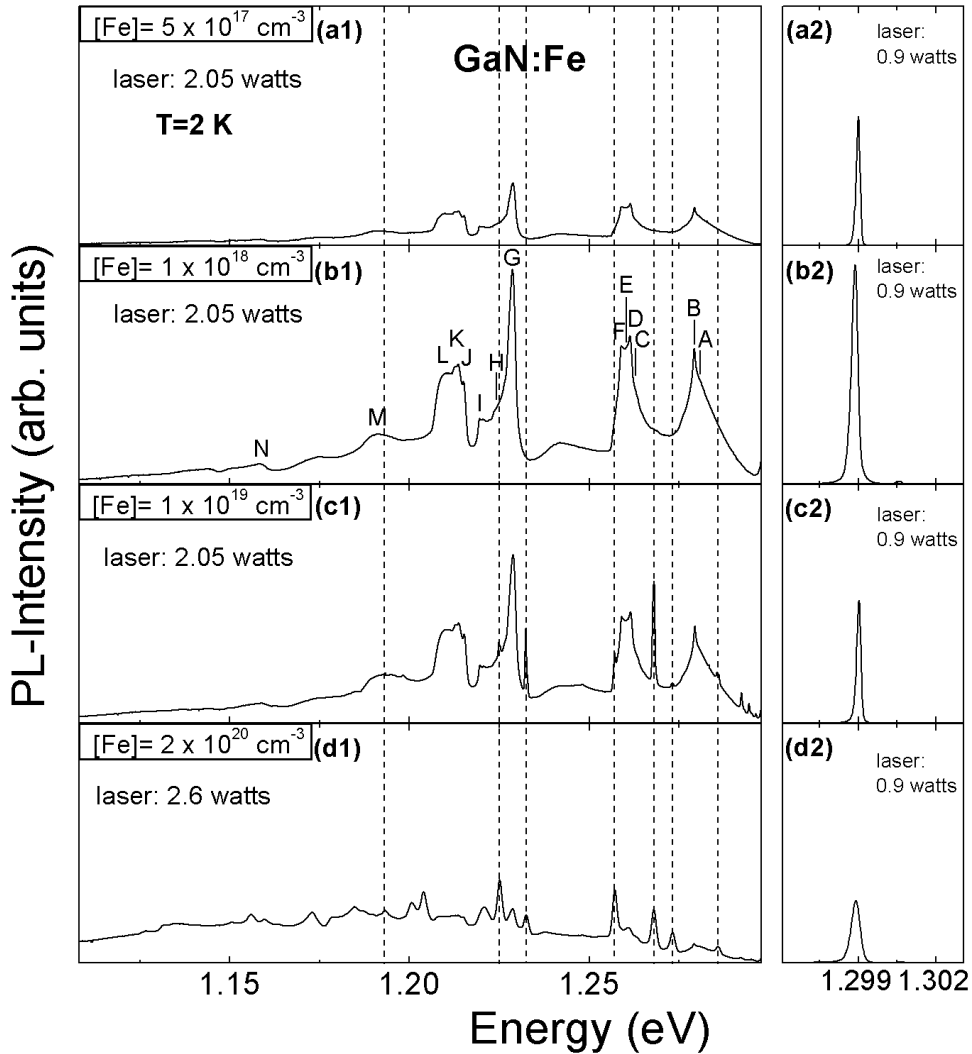


FIG. 2: Low-temperature (2 K) luminescence of the  $\text{Fe}^{3+}({}^4\text{T}_1(\text{G})\text{—}{}^6\text{A}_1(\text{S}))$  transition in GaN for different Fe concentrations. Excitation at 2.412 eV. Stated laser intensity is output power. The dominating ZPL at 1.299 eV is displayed at a different energy scale for better resolution. All spectra are displayed on the same intensity scale for quantitative comparison. ZPLs developing with increasing Fe concentration due to the formation of Fe-complexes are indicated by dashed lines. Capital letters in spectrum (b1) indicate lattice phonon replicas.

for Fe concentrations above  $1 \times 10^{19} \text{ cm}^{-3}$  (Fig. 2(c1) and (d1)), while spectra Fig. 2(a1) and (b1) consist of only the local vibrational modes (LVMs) and phonon modes.<sup>9,11</sup> In this spectral region, in previous studies on the  $\text{Fe}^{3+}$  center, further lines were observed which could be successfully assigned to the presence of other transition metal centers such as  $\text{V}^{3+}$ ,  $\text{Cr}^{4+}$ ,  $\text{Ti}^{2+}$  or  $\text{Co}^{2+}$ .<sup>8–10,20–22</sup> The absence of those lines in our spectra suggests that our Fe doped GaN samples are of high purity.

For a detailed analysis of the vibronic coupling of the  $\text{Fe}^{3+}$  center, the replicas observed for low Fe concentrations (Fig. 2(b1)) are compiled in Table II including their favored polarization (polarized spectra not shown). Their energies are compared to phonon modes of the host lat-

tice<sup>23,24</sup> and to LVMs.<sup>25,26</sup> We observe a strong coupling on the  $\text{E}_2$  phonon modes and  $\text{A}_1$  and  $\text{E}$  LVMs. The nature of the very strong replica at 19.8 meV, which has been detected before and interpreted as the actual  $\text{E}_2(\text{low})$  phonon,<sup>22</sup> is still unclear.

The energy of the  $\text{E}_2$  phonon mode is sensitive to lattice strain.<sup>27</sup> Therefore, measuring the energetic distance between the ZPL and an  $\text{E}_2$  replica provides a way to probe the local strain induced by the iron incorporation. The energy of the  $\text{E}_2(\text{high})$  phonon mode remains constant (70.1 meV) with varying Fe concentration (Fig. 5(c)), confirming the relatively stress free incorporation of iron, even for concentrations as high as  $2 \times 10^{20} \text{ cm}^{-3}$ . This result was confirmed by determining the energy of the  $\text{E}_2(\text{high})$  phonon mode using Raman

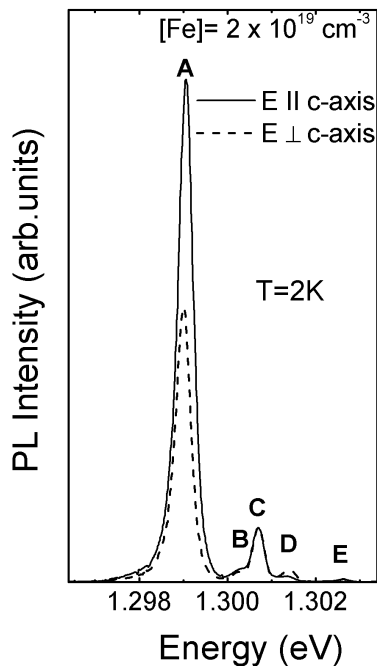


FIG. 3: Polarized high resolution PL spectra of the ( ${}^4T_1(G)$ — ${}^6A_1(S)$ ) ZPL of  $Fe^{3+}$  in GaN at  $T=2$  K,  $[Fe]=1\times 10^{19}$   $cm^{-3}$ . At an excitation power of 4 watts (output), transitions involving higher  ${}^4T_1(G)$  sub-levels appear on the high-energy side of the ZPL at 1.299 eV.

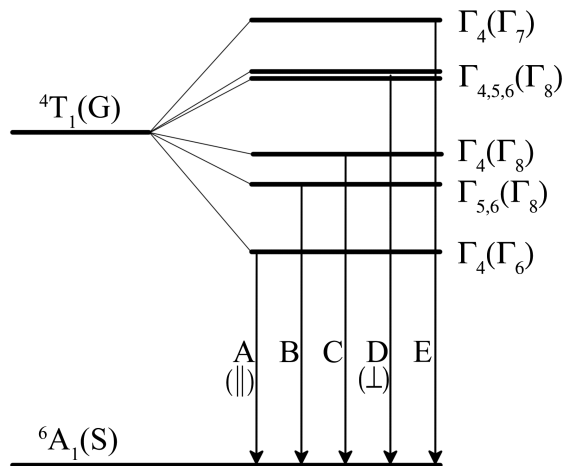


FIG. 4: Splitting of the  ${}^4T_1(G)$  state in trigonal  $c_{3v}$  symmetry, derived from the fine-structure of the ( ${}^4T_1(G)$ — ${}^6A_1(S)$ ) luminescence (Fig. 3). The original symmetries resulting from only spin-orbit coupling are given in brackets. Observed transitions and their respective polarization are indicated by arrows. Letters refer to the PL spectrum Fig. 3.

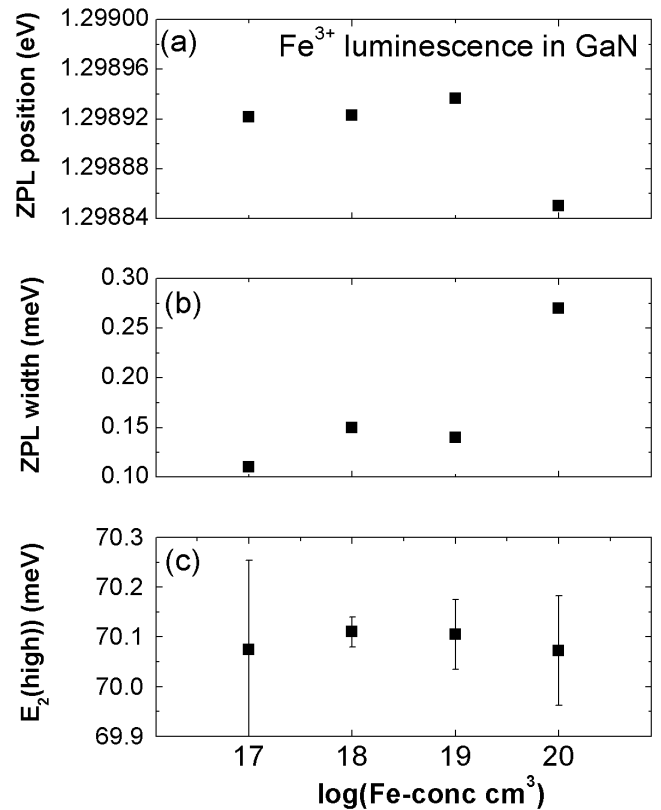


FIG. 5: Concentration dependency of the  $Fe^{3+}({}^4T_1(G)$ — ${}^6A_1(S))$  luminescence: (a) position of the ZPL, (b) FWHM of ZPL and (c) energy of  $E_2$  phonon mode.

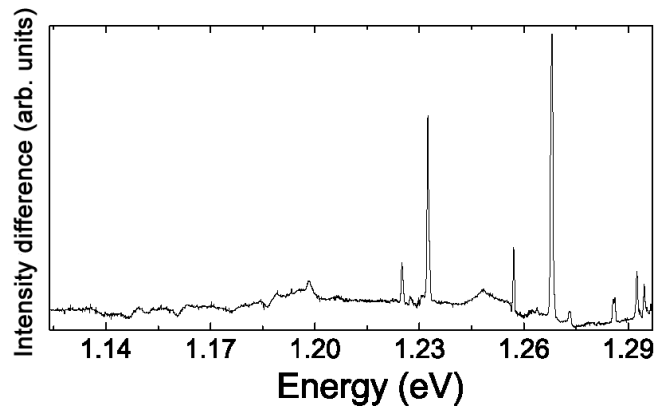


FIG. 6: PL difference spectrum of the sideband of the  $Fe^{3+}$  emission in GaN. In Fig. 2 the spectrum (a1) was subtracted from spectrum (c1) revealing the Fe-complex lines.

scattering (measurements not shown).

The additional sharp lines which appear within the sideband for high Fe concentrations (Fig. 2(c1) and (d1)) have been observed before and were attributed to the formation of defect complexes involving iron.<sup>8,14,28</sup> This assignment is supported by the fact that the intensity of the lines in question scales with the Fe concentration.

TABLE II: Sideband of  $\text{Fe}^{3+}$  ( ${}^4\text{T}_1(\text{G})\text{—}{}^6\text{A}_1(\text{S})$ ) luminescence. Listed are the replicas as seen for  $[\text{Fe}]=5\times 10^{18}\text{ cm}^{-3}$  in Fig. 2(b1) and their favored polarization.  $\Delta\text{E}$  is the energetic distance from the ZPL at 1.299 eV. Moreover, possible phonon modes<sup>23,24</sup> and LVMS<sup>25,26</sup> including their energies are given in the last three columns.

Line	E (eV)	$\Delta\text{E}$ (meV)	Polarization	$\hbar\omega$ (meV)	Vibrational mode	Ref.
A	1.28110	17.9		17.80	$\text{E}_2(\text{low})$	23
B	1.27920	19.8				
C	1.26290	36.1		A+A		
D	1.26150	37.5		37.30	LVM ( $\text{A}_1$ )	25
E	1.25980	39.2		39.20	LVM ( $\text{A}_1$ )	25
F	1.25910	39.9		39.55	$\text{B}_1(\text{low})$	24
G	1.22890	70.1	$\perp$	70.50	$\text{E}_2(\text{high})$	23
H	1.22415	74.8	$\perp$	D+D or 75.10	LVM $\text{A}_1$	26
I	1.21960	79.4	$\perp$			
J	1.21520	83.8				
K	1.21380	85.2	$\perp$	85.50	LVM ( $\text{A}_1$ )	25
L	1.20995	89.0		88.90	LVM ( $\text{E}$ )	25
M	1.19140	107.6		D+G		
N	1.15830	140.7		G+G		

Fig. 6 shows the spectrum of only the additional lines. It was derived by subtracting the phonon and LVM spectrum Fig. 2(a1) from the sideband including the defect lines Fig. 2(c1).

The most pronounced line at 1.268 eV with a FWHM of  $580\text{ }\mu\text{eV}$  is attributed to a complex involving a donor, ( $\text{Fe}^{3+}$ , D+), on the basis of PLE spectra which can be explained with the  $\text{Fe}^{3+}$  term scheme considering the presence of additional excitation mechanisms.<sup>28</sup> Further similarities to the luminescence of the isolated  $\text{Fe}^{3+}$  center are a long lifetime indicating a spin-forbidden transition

TABLE III: Sharp lines associated with Fe-complexes and their polarization. Only the ZPL at 1.268 eV and lines at smaller energies are listed. Possible phonon modes<sup>23</sup> and LVMS<sup>25</sup> are given in the last column including their energies.

Line (eV)	Polarization	$\Delta\text{E}$ (meV)	$\hbar\omega^2$ (meV)	Vibrational mode
1.2681	$\perp$			
1.2638		4.3		
1.2571		11.0		
1.2483		19.8		
1.2324	$\perp$	35.7	37.3	LVM ( $\text{A}_1$ )
1.2250		43.1	39.2	LVM ( $\text{E}$ )
1.1983		69.8	70.50	$\text{E}_2(\text{high})$
1.1933		74.8	$2\times 37,3$	

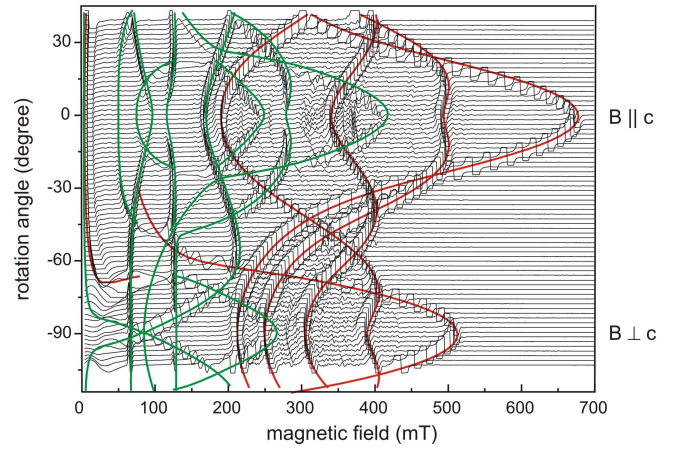


FIG. 7: EPR spectra of Fe doped GaN,  $[\text{Fe}]=1\times 10^{19}\text{ cm}^{-3}$ , 9.49 GHz and 4 K. Stackplot for rotation of the magnetic field ( $5^\circ$  step width) from  $\text{B}\parallel\text{c}$ -axis to  $\text{B}\perp\text{c}$ -axis. In this graph, the five allowed transitions ( $\Delta\text{M}=\pm 1$ ) of  $\text{Fe}^{3+}$  with  $\text{S}=\frac{5}{2}$  are observed with strong intensity, while the forbidden transitions ( $\Delta\text{M}=\pm 2, \pm 3, \pm 4, \pm 5$ ) appear as weak resonances. Theoretical line positions were calculated for allowed (red curve) and forbidden (green curve) transitions using the corresponding spin Hamiltonian for  $\text{Fe}^{3+}$  in GaN and the parameters given in Ref. 15. Additional weak transitions mainly originate from  $\text{Fe}^{3+}\text{—Ga}$  pairs.

and the observation of higher levels of the excited state at high temperatures.<sup>28</sup> However, a strongly modified electronic structure is suggested by the Zeeman-behavior not showing the fingerprint of a  $d^5$ -configuration.<sup>28</sup>

Table III summarizes lines of higher energies and points out possible vibronic replica of the 1.268-eV line. This association is supported by identical PLE spectra at least for the lines at 1.2324 and 1.1933 eV. Basically, a coupling with the same phonon and local vibrational modes as for the 1.299-eV line is observed. Differences particularly regarding the LVM energies are plausible as the neighborhood of the  $\text{Fe}^{3+}$  center as part of a complex differs from that of the isolated  $\text{Fe}^{3+}$  center. It should be noted that the replica at 1.193 eV is found at the same position as the  $\text{Ti}^{2+}$  luminescence in GaN specimens of poorer purity.<sup>29</sup>

Further lines in Fig. 6 must be ZPLs themselves or replicas of one. Obviously, iron forms different complexes with other defects. Their exact nature still remains unclear. As mentioned above, complexes involving donors, e.g. nitrogen vacancies or oxygen, have been suggested as the origin of the additional lines under discussion.<sup>14,28</sup> However, that does not quite explain the strong dependence on the Fe concentration. From this perspective Fe-Fe complexes are more plausible.

An additional fingerprint of  $\text{Fe}^{3+}$ -related defect complexes in heavily Fe-doped GaN comes from angular-dependent EPR spectra, as illustrated in Fig. 7. The dominant lines with strong intensity originate from allowed transitions ( $\Delta\text{M}=\pm 1$ ) of isolated  $\text{Fe}^{3+}$  centers.

TABLE IV: Absorption lines found in UV-VIS-Transmission spectra at 2 K with the polarization given in brackets.  $\Delta E$  refers to the last value of the group above. Possible assignments are given in the right column.

Absorptionline (meV)	$\Delta E$ (meV)	Assignment
2.0172 (  )		( ${}^4T_2(G)$ — ${}^6A_1(S)$ )
2,7247		( ${}^4E(G)$ — ${}^6A_1(S)$ )
2,7244 ( $\perp$ )	-0,3	( ${}^4E(G)$ — ${}^6A_1(S)$ )
2,7258 (  )	1,1	( ${}^4E(G)$ — ${}^6A_1(S)$ )
2,812	87	ZPL of ( $(Fe^{2+},h)$ — ${}^6A_1(S)$ )
2,836	24	
2,849	37	LVM ( $A_1$ ) of ZPL
2,884	72	$E_2(\text{high})$ or LVM $A_1$
2,908	24	
2,922	38	( $E_2$ or $A_1$ ) + $A_1$
2,957	73	$2 \times (E_2$ or $A_1)$
2,981	24	
2,995	38	$2 \times (E_2$ or $A_1) + A_1$
3,030	73	$3 \times (E_2$ or $A_1)$

Also, due to the relatively large zero-field splitting of  $D = -0.0768 \text{ cm}^{-3}$  and the corresponding strong mixing of wavefunctions, several forbidden transitions ( $\Delta M = \pm 2, \pm 3, \pm 4, \pm 5$ ) of lower intensity are observed. A characteristic of forbidden transitions is the vanishing of the respective lines in the main crystal directions, i.e.  $B \parallel c$ -axis or  $B \perp c$ -axis, as shown in Fig. 7. The theoretically calculated angular dependencies of the EPR peaks are indicated in Fig. 7 by red (allowed transitions) and green (forbidden transitions) lines. Apart from the lines attributed to isolated  $Fe^{3+}$  centers, additional weak transitions are detected, which support the optical observation of  $Fe^{3+}$ -related defect complexes. Most of these lines appear as weak satellites of the dominant  $Fe^{3+}$  transitions and are attributed to  $Fe^{3+}_{Ga} - Ga_i$  pairs.<sup>30</sup> In wurtzite lattice structure, there are 12 possible center orientations of these pairs leading to the observed multitude of lines. The most prominent of those lines originate from centers with the principal axis in parallel with the  $c$ -axis and are analyzed in Ref. 30. A few very weak lines cannot be attributed to  $Fe^{3+}_{Ga} - Ga_i$  pairs and might in fact originate from Fe-Fe pairs.

### C. UV-VIS Transmission Spectroscopy

The transmission spectra in Fig 8 reveal higher excited  $Fe^{3+}$  states for Fe concentrations from  $1 \times 10^{18} \text{ cm}^{-3}$ . The main absorption features are compiled and assigned in Table IV. Transitions into the excited  $Fe^{3+}$  states

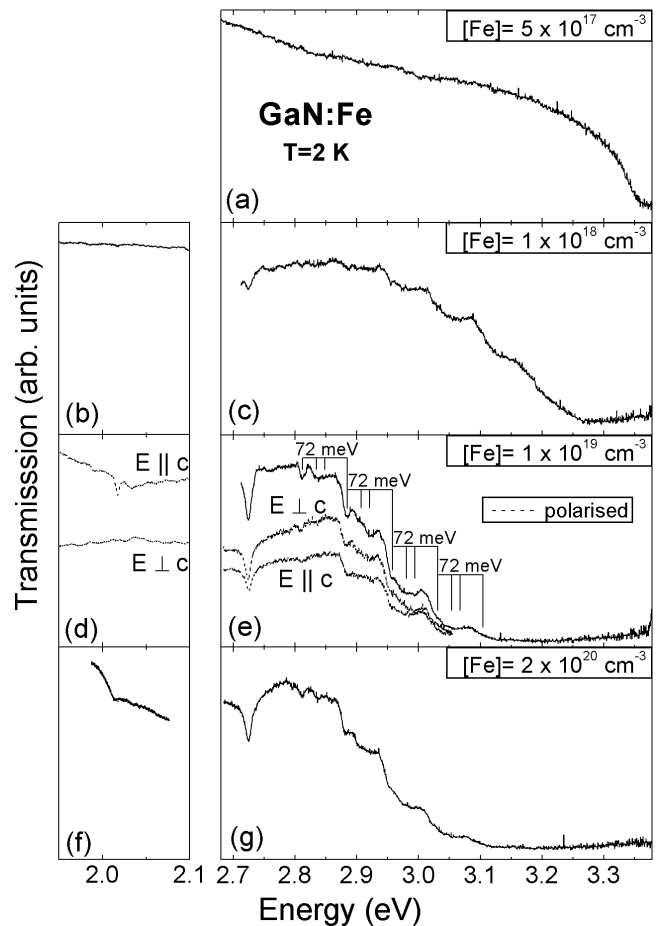


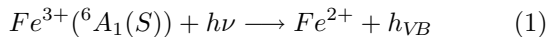
FIG. 8: Optical transmission spectra of Fe-doped GaN with different concentrations of iron at 2 K using a xenon lamp. Irradiating perpendicular to the  $c$ -axis the path length through the sample was  $\sim 2$  mm. Polarized measurements are only presented for an iron-content of  $1 \times 10^{19} \text{ cm}^{-3}$ . The step-like structure associated with the effective-mass-like state at 2.812 eV is indicated for  $[Fe] = 1 \times 10^{19} \text{ cm}^{-3}$ .

${}^4T_2(G)$  and  ${}^4E(G)$  appear as peaks at 2.0172 eV and 2.7247 eV, respectively.<sup>8</sup> The observed weak phonon coupling is typical for intra-center transitions.<sup>31</sup> The relatively large FWHMs of 2.8 meV and 7.4 meV (for  $[Fe] = 1 \times 10^{19} \text{ cm}^{-3}$ ), respectively, is natural and not due to limited spectral resolution. The ( ${}^4T_2(G)$ — ${}^6A_1(S)$ ) absorption (Fig. 8(d)) exhibits an pronounced polarization ( $E \parallel c$ -axis). Polarized spectra also yield a splitting of the ( ${}^4E(G)$ — ${}^6A_1(S)$ ) peak (Fig. 8(e)). Apparently, the splitting of the  ${}^4E(G)$  state is too small to be resolved with a linewidth as this large. Consequently, the  ${}^4E(G)$  state splits at least into a doublet with a magnitude of 1.4 meV. However, further unresolved splitting cannot be ruled out making conclusions about the Jahn-Teller coupling of the  ${}^4E(G)$  state impossible. The ( ${}^4T_2(G)$ — ${}^6A_1(S)$ ) absorption at 2.0172 eV has been intensively investigated by Heitz et al. using high resolution PLE. A fourfold structure was resolved with the lowest transition at 2.0091 eV

indicating a weak Jahn-Teller coupling due to the hexagonal host lattice.<sup>8</sup>

A peak at 2.812 eV yields a strong phonon coupling which appears as a step-like structure and is indicated in Fig. 8(e). What Heitz et al. identified as a bound state consisting of an exciton bound to  $\text{Fe}^{3+}$ , ( $\text{Fe}^{3+}, e, h$ ), is in fact the first replica at 2.884 eV.<sup>8</sup> Table IV lists the replicas and possible candidates of their origin. By comparing the energies of phonon and local vibrational modes, there are three possible explanations for the most pronounced replicas with an energy between 72 and 73 meV: (i) The combination of two  $A_1$  LVMs of 37.3 meV<sup>25</sup> each is unlikely since the replica at this value is unequally weaker. (ii) An  $A_1$  LVM of 75.10 meV<sup>26</sup> and (iii) an  $E_2$  (high) phonon mode of 70.50 eV<sup>23</sup> both deviate from the experimentally found value by about 2 meV. While the energy of the resonance between 37 and 38 meV (see table IV) perfectly agrees with the  $A_1$  LVM of 73.3 meV,<sup>25</sup> the origin of the replica at 24 meV is still unclear.

The step-like structure is the result of the bound state's replica super imposed on the start of a broad absorption band occurring in the UV spectral region. This band represents the  $\text{Fe}^{3+/2+}$  charge transfer (CT) process



in which a hole is excited into the valence band.<sup>8</sup> The CT band's low energy onset equals the position of the  $\text{Fe}^{3+/2+}$  CT level within the band gap as measured from the valence band maximum. An exponential fit narrows it down to  $2.863 \pm 5$  eV. Heitz et al. could not accept this value, since it is below of what they believed to be the bound state. Instead the CT level was thought to be at  $3.17 \pm 0.1$  eV.<sup>8</sup> The new position of the CT level brings the following implications upon the bound state: With the CT level further away from the CB  $0.68 \pm 0.06$  eV, only a minor hybridization of the Fe ion's core states with the CB needs to be taken into account. In addition, since the binding energy is only  $(50 \pm 10)$  meV, the hole is bound less tightly producing a smaller overlap between the hole and the core wavefunctions. Both effects lead to a weak exchange interaction between the hole and the core states. Consequently, the bound state is of the same character the Fe acceptor in other III-V materials, which is best described as a hole bound to an  $\text{Fe}^{2+}$  center ( $\text{Fe}^{2+}, h\nu_B$ ).<sup>18,32,33</sup>

This shallow bound state can be described as an effective-mass-like complex with a Coulomb interaction. It constitutes a transient shallow acceptor state and represents the highest excited state of the  $\text{Fe}^{3+}$  center. A bound state of the form ( $\text{Fe}^{2+}, h\nu_B$ ) would also explain the deviation from the LVM energy that was originally calculated and measured for the  $\text{Fe}^{3+}$  ground state.<sup>26</sup> As a result, the  $A_1$  LVM discussed above is probably the cause of the replica with an energy between 72 and 73 meV.

High resolution transmission spectra of the 2.812-eV line (not shown here) yield a threefold splitting of a magnitude of approximately 8 meV. This observation

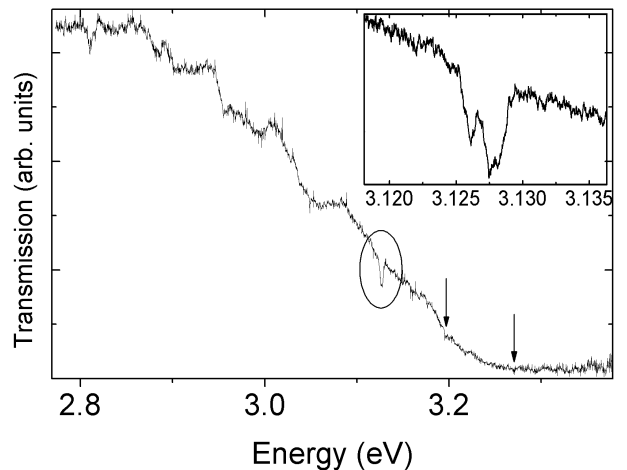


FIG. 9: Optical UV transmission spectrum of GaN with  $[\text{Fe}] = 1 \times 10^{19} \text{ cm}^{-3}$  at 2 K and  $\vec{k} \parallel c$ -axis. A sharp absorption feature is detected peaking around 3.127 eV. The arrows indicate possible phonon replicas of  $\sim 72$  meV. The inset shows a high-resolution spectrum of the encircled area.

is in good agreement with findings in GaAs, GaP and InP where the core wavefunctions, though influenced by the loosely bound hole, are well localized at the  $\text{Fe}^{2+}$  ion.<sup>18,32,33</sup> Consequently, the fine structure of the  $\text{Fe}^{2+}({}^5E)$  state is indicated by the observed splitting. In fact, the  ${}^5E$  state of cubic lattice types bears five sub-levels. However, even in high resolution calorimetric absorption spectroscopy (CAS) of Fe doped InP and GaP only three lines are well resolved.<sup>32</sup>

Under the influence of the axial distortion of the tetrahedral crystal field ( $c_{3V}$  symmetry) the  $\text{Fe}^{2+}({}^5E)$  state is shown to further split into at least seven sub-levels.<sup>13</sup> Apparently, only three of those are resolved in form of the fine structure of the bound state. The factor between the splitting observed here and the splitting of the  $\text{Fe}^{2+}({}^5E)$  state is roughly 2 which agrees with findings for the same state in InP and GaP.<sup>13,32</sup>

Figure 9 shows a transmission spectrum which was recorded with the  $c$ -axis parallel to the optical path resulting in an absorption pathlength of  $400 \mu\text{m}$ . Besides the discussed effective-mass-like state at 2.812 eV, it shows another absorption feature of multifold structure around 3.127 eV. In analogy to the 2.812-eV peak representing a hole bound to the  $\text{Fe}^{2+}$  ground state,  ${}^5E$ , we tentatively assign this feature to a hole bound to the excited state of  $\text{Fe}^{2+}$ ,  ${}^5T_2$ . Equivalent transitions have been identified successfully for  $\text{Fe}^{2+}$  in GaAs, GaP and InP.<sup>18,34,35</sup> The assumption is supported by the observed splitting, reflecting the fine structure of the  $\text{Fe}^{2+}({}^5T_2)$  state and by the steps in Fig. 9 at 3.1974 and 3.2707 eV (arrows). As with the ( $\text{Fe}^{2+}({}^5E), h\nu_B$ ) state, the latter are the replica on account of the discussed  $A_1$  LVM or  $E_2$ (high) phonon mode with an energy of 73 meV. The spacing between the two discussed bound states amounts



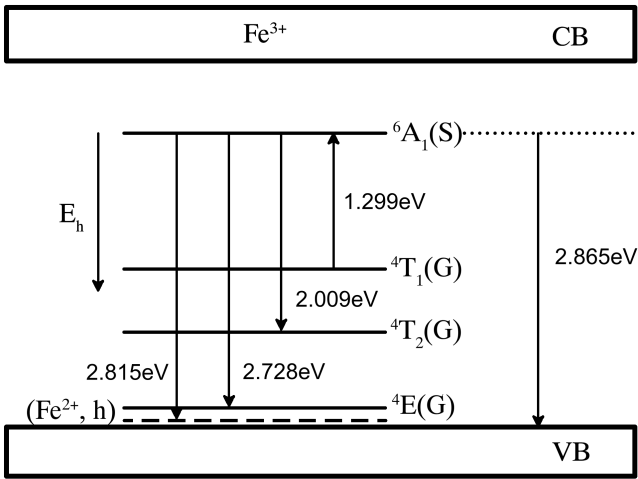


FIG. 10: Term scheme of  $\text{Fe}^{3+}$  in GaN. The  ${}^4\text{G}$  state is split by the crystal field into the ground state  ${}^6\text{A}_1(\text{S})$  and the excited states  ${}^4\text{T}_1(\text{G})$ ,  ${}^4\text{T}_2(\text{G})$  and  ${}^4\text{E}(\text{G})$ . Further excitation leads to a shallow bound state (binding energy of  $(50 \pm 10)$  meV). Transitions between these states are described best in the hole-picture as indicated by the arrow on the left hand side. Transitions observed in transmission experiments are indicated by arrows.

to 315 meV. However, the energy of the ( ${}^5\text{E}-{}^5\text{T}_2$ ) transition of the  ${}^5\text{D}$  states of  $\text{Fe}^{2+}$  is shown to be 385 meV later on in this work. As a result, the binding energy of the effective-mass-like state involving the excited  ${}^5\text{E}$  state of  $\text{Fe}^{2+}$  would have a 70 meV higher binding energy than the one discussed before. For the host materials GaAs, GaP and InP these respective energies are equal.<sup>18,34,35</sup> Therefore, it is possible that the peak at 3.1275 eV is caused by impurities originating from the substrate. This assumption is supported by the fact that the absorption line at 3.1275 eV was only detected for the light traveling parallel to the  $c$ -axis.

In summary, all absorption features found by VIS-UV transmission experiments (Fig. 8) were assigned to internal transitions within the  $\text{Fe}^{3+}$  center. Since none of those features was observed for a Fe concentration of  $5 \times 10^{17} \text{ cm}^{-3}$  (Fig. 8(a)), it can be concluded that at this concentration no Fe ions are present in the 3+ charge state. The cause is the position of the Fermi level above the  $\text{Fe}^{3+/2+}$  CT level. As discussed above, only with increased Fe concentration residual n-type conductivity is compensated by Fe acceptors, eventually lowering the Fermi level deep enough for  $\text{Fe}^{3+}$  centers to stay un-ionized. Consequently, the  $\text{Fe}^{3+}$  luminescence in Fig. 2(a2) for low Fe concentrations must be excited via a different channel than intra-center transitions.

Figure 10 illustrates the term scheme of  $\text{Fe}^{3+}$  in GaN on the basis of the just outlined findings rectifying the one established by Heitz et al.<sup>8</sup> The most important points are the position of the CT level at  $2.863 \text{ eV} \pm 5 \text{ meV}$  above the valence band and the binding energy of the pseudo-acceptor ( $\text{Fe}^{2+}$ ,  $h_{\text{VB}}$ ) of  $(50 \pm 10)$  meV. The im-

plications of the position of the CT level regarding the applicability of the internal reference rule<sup>6,7</sup> for the prediction of band off-sets in semiconductor heterojunctions (HJ) are: For the GaN/GaAs HJ, a valence band discontinuity of  $1.84 \pm 0.1 \text{ eV}$  has been established by ultraviolet photoemission spectroscopy (UPS) and first principle calculations.<sup>36,37</sup> However, our results suggest a type-I band alignment with a valence band off-set of 2.4 eV. Obviously, the internal reference rule cannot be used to predict band discontinuities between GaN and other III-V materials. The reason probably relates to the exceptionally large electronegativity of nitrogen in comparison to other group-V elements.

No conclusion about the validity of the internal reference rule for the GaN/AlN material system can be drawn. By means of x-ray photoemission spectroscopy (XPS) a type-I lineup with a valence band discontinuity of  $0.7 \pm 0.24 \text{ eV}$  has been found.<sup>38</sup> However, the only literature about the  $\text{Fe}^{3+/2+}$  level in AlN is based on an inaccurate experimental methodology, which results in a large experimental error.<sup>20</sup> Assuming the internal reference rule holds for the GaN/AlN HJ, our results suggest the CT level in AlN to be 2.6 eV below the conduction band.

An additional consequence of the  $\text{Fe}^{3+/2+}$  CT level being located  $0.68 \pm 0.06 \text{ eV}$  below the conduction band is that the  $\text{Fe}^{2+}({}^5\text{E}-{}^5\text{T}_2)$  transition might be located within the band gap. This transition was previously believed to be absent, since the CT level was thought to be 0.33 eV below the conduction band and, with typical ( ${}^5\text{E}-{}^5\text{T}_2$ ) transition energies of 0.35 - 0.40 eV, the  ${}^5\text{T}_2$  level might degenerate with the conduction band. Indeed, in agreement with the deeper  $\text{Fe}^{3+/2+}$  CT level, the existence of the  $\text{Fe}^{2+}({}^5\text{E}-{}^5\text{T}_2)$  transition could be shown by IR transmission experiments as illustrated in the following section.

#### D. FTIR Transmission Spectroscopy

In Fig. 11(b), FTIR spectra of the set of Fe doped GaN samples exhibit a richly structured absorption band at around 395 meV. We assign this feature to the internal ( ${}^5\text{E}-{}^5\text{T}_2$ ) transition of  $\text{Fe}^{2+}$  on the basis of three reasons: (i) The observed absorption structure is found in the same energetic region and is of similar shape as the same transition in GaAs, GaP and InP, i.e. between 340 and 450 meV.<sup>12</sup> For comparison, the spectrum of the ( ${}^5\text{E}-{}^5\text{T}_2$ ) transition in GaP recorded by the same experimental setting is displayed in Fig. 11(a). (ii) The shape and amplitude of the absorption changes significantly with the Fe concentration. (iii) PLE spectra presented below yield a second CT band at a distance from the first one equal to the position of the absorption feature in question.

The  $\text{Fe}^{2+}$  ion represents a  $d^6$  configuration. In the trigonal ligand field of  $T_d$  symmetry in a cubic (zinc blende) host lattice, the  ${}^5\text{D}$  ground state splits into a  ${}^5\text{E}$  ground

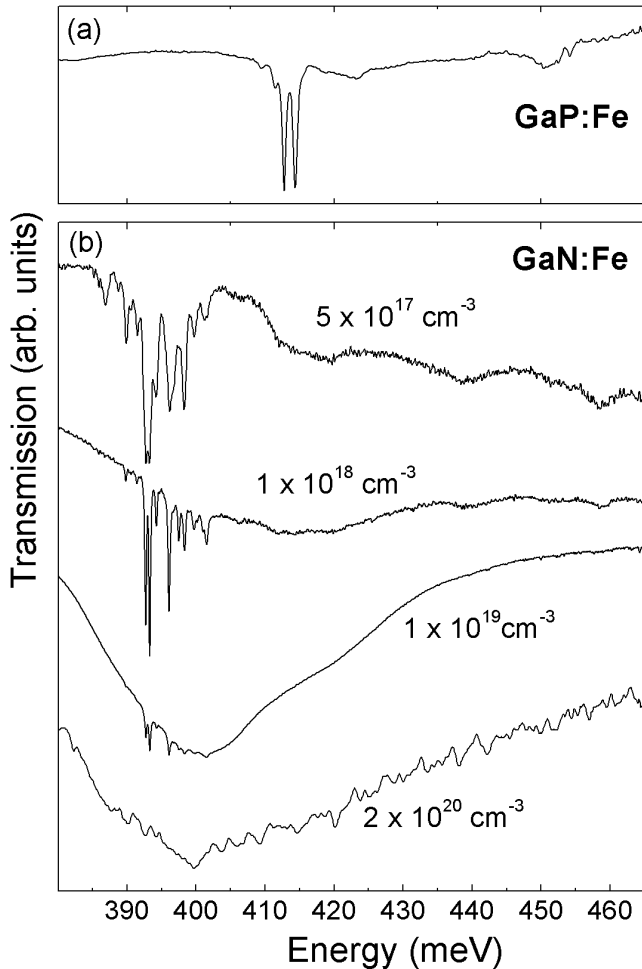


FIG. 11: FTIR transmission spectra of (a) Fe doped GaP and (b) Fe doped GaN showing the richly structured  $\text{Fe}^{2+}$  ( ${}^5\text{E} \rightarrow {}^5\text{T}_2$ ) transition in both materials at  $T \approx 40$  K. The noisy signal for  $[\text{Fe}] = 2 \times 10^{20} \text{ cm}^{-3}$  is the result of the very high overall absorption of this sample.

state and a  ${}^5\text{T}_2$  excited state. Spin-orbit-interaction causes the  ${}^5\text{E}$  and  ${}^5\text{T}_2$  states to split into 5 and 6 sub-levels, respectively. This splitting can be used to explain the  $\text{GaP}:\text{Fe}^{2+}$  spectrum in Fig. 11(a) taking into account a strong Jahn-Teller coupling, the thermal population of the ground states as well as selection rules.<sup>12,33,39</sup> The spectra of the ( ${}^5\text{E} \rightarrow {}^5\text{T}_2$ ) transition in GaN (Fig. 11(b)) are more complex because of an additional splitting due to the axial distortion of the crystal field in  $c_{3V}$  symmetry. The precise assignment of the observed transitions and the determination of the  $\text{Fe}^{2+}$  term scheme will be presented in a separate paper.<sup>13</sup> We have observed a similar transition in Fe doped ZnO, which is currently the topic of further study.

With increasing Fe concentration, a broad absorption band develops at the position of the  $\text{Fe}^{2+}$  transitions at around 400 meV that probably results from an inter-center interaction that causes the single ( ${}^5\text{E} \rightarrow {}^5\text{T}_2$ ) lines

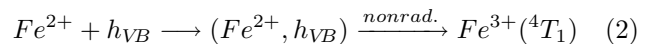
to broaden.

Since the ( ${}^5\text{E} \rightarrow {}^5\text{T}_2$ ) transition is present in all spectra of Fig. 11(b), we can assume that  $\text{Fe}^{2+}$  is a stable charge state at any Fe concentration. A dynamic process in which  $\text{Fe}^{2+}$  is only created from present  $\text{Fe}^{3+}$  can be ruled out because the specimens were not exposed to light of sufficient energy (2.865 eV) to accomplish the  $\text{Fe}^{3+/2+}$  charge transfer process. Consequently, we conclude that the Fermi level does not drop below the  $\text{Fe}^{3+/2+}$  charge transfer level at 2.865 eV, leading to a coexistence of  $\text{Fe}^{3+}$  and  $\text{Fe}^{2+}$  at high Fe concentrations.

As mentioned before,  $\text{Fe}^{2+}$  was not detected by EPR. A possible explanation for this discrepancy between optical and magnetic experiments is the fact that  $\text{Fe}^{2+}$  ( $d^6$ -configuration) is a non-Kramers-ion and therefore difficult to detect by EPR.

### E. PL Excitation

In order to gain further insights regarding the excitation and CT processes in Fe doped GaN, PLE studies of the  $\text{Fe}^{3+}({}^4\text{T}_1(\text{G}) \rightarrow {}^6\text{A}_1(\text{S}))$  luminescence were conducted. The detection window was set to a 8 meV wide window around 1.299 meV. Figure 12 illustrates PLE measurements for different Fe concentrations. The spectra show similar features to those observed in transmission experiments: Internal transitions into the excited  $\text{Fe}^{3+}$  states  ${}^4\text{T}_2(\text{G})$ ,  ${}^4\text{E}(\text{G})$  and the effective-mass-like state for Fe concentrations from  $1 \times 10^{18} \text{ cm}^{-3}$ . The vibronic sideband of the  ${}^4\text{T}_2(\text{G})$  transition was analyzed in detail by Heitz et al. and indicates a dynamic Jahn-Teller effect.<sup>8</sup> The presence of the  $\text{Fe}^{3+/2+}$  CT band starting at  $2.865 \pm 0.008$  meV suggests that the CT process initiates a very efficient excitation mechanism of the  $\text{Fe}^{3+}$  center. This excitation process is described in detail by the following equation.



Following the  $\text{Fe}^{3+/2+}$  CT process (Equation 1) the free hole is captured by a  $\text{Fe}^{2+}$  center probably by first forming the discussed bound ( $\text{Fe}^{2+}, h\nu_{\text{VB}}$ ) state, which then relaxes nonradiatively into the  $\text{Fe}^{3+}({}^4\text{T}_1(\text{G}))$  state. The position of the CT band observed here is in good agreement with the results of the transmission spectra (Fig. 8). A second excitation band can be seen, particularly for  $[\text{Fe}] = 2 \times 10^{20} \text{ cm}^{-3}$  in Fig. 12(d2), starting at  $3.245 \pm 0.02$  eV. The difference between the two onsets,  $380 \pm 20$  meV, equals the splitting of the  ${}^5\text{D}$  state of  $\text{Fe}^{2+}$  established by FTIR measurements. Consequently, the second band represents the CT process process resulting in the  $\text{Fe}^{2+}$  state,  ${}^5\text{T}_2$ .

The spectra presented in Figs. 12(b2)-(d2) suggest that the capture of free holes by  $\text{Fe}^{2+}$  centers is the most efficient excitation mechanism of  $\text{Fe}^{3+}$ . GaN samples with Fe concentrations of  $1 \times 10^{18} \text{ cm}^{-3}$  and  $5 \times 10^{17} \text{ cm}^{-3}$  exhibit weak or no  $\text{Fe}^{3+}$  related features, respectively.

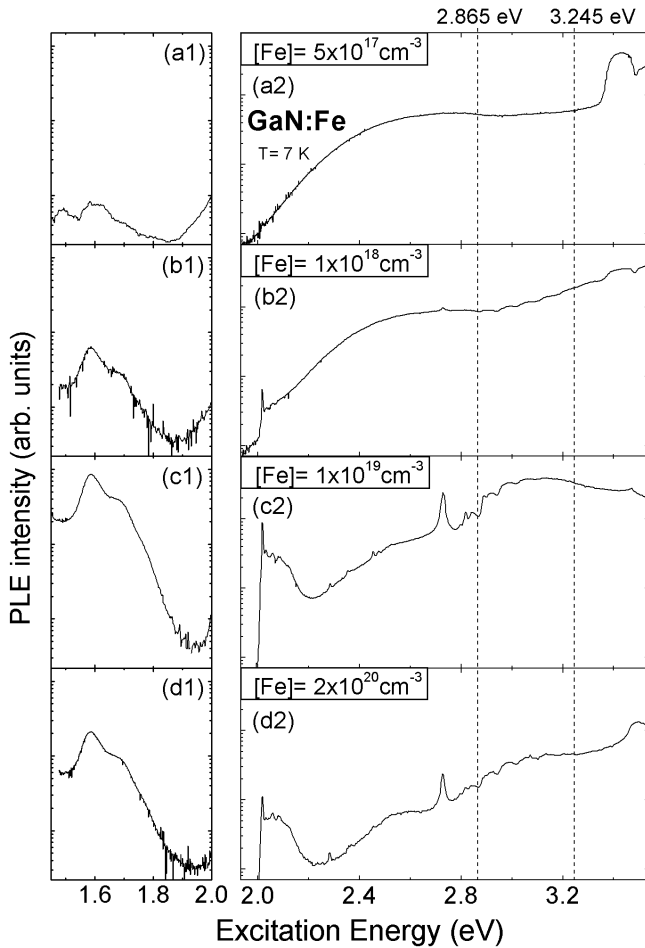


FIG. 12: PLE spectra of the  $\text{Fe}^{3+}({}^4\text{T}_1(\text{G})\text{—}{}^6\text{A}_1(\text{S}))$  luminescence at 1.299 eV of Fe doped GaN at 7 K on logarithmic scale. The luminescence was detected in an 8 meV wide window around 1.299 eV. All spectra in one column are displayed on the same intensity scale. The dashed lines mark the onsets of excitation bands representing CT processes resulting in the  $\text{Fe}^{2+}$  states  ${}^5\text{E}$  and  ${}^5\text{T}_2$ .

Nevertheless, they show the  $\text{Fe}^{3+}$  luminescence at the same intensity as higher doped samples and, according to FTIR experiments, they definitely contain  $\text{Fe}^{2+}$ . Therefore, at low Fe concentrations, holes must be provided via different channels. Excitation processes of the  $\text{Fe}^{3+}$  luminescence by hole transfer from other impurities to  $\text{Fe}^{2+}$  centers are known from n-type II-VI semiconductors, e.g. ZnO and ZnS.<sup>16,19</sup> In ZnS,  $\text{Cu}^{2+}$  is a well established source of free holes.<sup>16</sup> By means of PLE and two color stimulation, Hoffmann et al. established a close correlation between the excitation processes of the  $\text{Fe}^{3+}$  center and the intrinsic yellow luminescence (YL) of n-type GaN.<sup>40</sup> According to Ref. 40, the ionization of natural defects forming deep double donors around 2.3 eV below the CB initiates the YL transition and, at the same time, represents the first step of a two step generation of free holes.<sup>41</sup> PLE spectra of the YL yield the

ionization process in form of the same excitation band starting at 2.1 eV as presented in Fig. 12.<sup>40</sup> Hence, the deep defects involved in the yellow luminescence can act as a hole source equally at any investigated Fe concentration, as the 2.1-eV band is present with equal intensity in all spectra of Fig. 12. Consequently, the quenching of the YL by the incorporation of iron<sup>42</sup> is merely accomplished by the lowered Fermi level, ionizing the shallow donor involved in the YL.<sup>41</sup> That also explains the equal intensity of the  $\text{Fe}^{3+}$  luminescence in Fig. 2 which was excited at 2.4 eV, where the dominating excitation process is the generation and subsequent capture of holes as outlined above. Apparently, the bottleneck of the  $\text{Fe}^{3+}$  excitation at this energy is not the density of Fe centers but the availability of hole sources (i.e. intrinsic deep defects) which is shown here to be independent of the Fe doping. The observation of the 2.1-eV band in all spectra presented in Fig. 12 also confirms the presence of  $\text{Fe}^{2+}$  even at high Fe concentrations in agreement with the FTIR spectra (Fig. 11) and the position of the Fermi level.

The near-band-gap excitation at 3.4 eV (Fig. 12(a2) and (b2)) is tentatively explained by a hole generation via the shallow donor state 35 meV below the CB involved in the YL.<sup>40</sup> This donor would be passivated at higher Fe concentrations.

The positions of the sharp minima at 3.484 eV for  $[\text{Fe}] = 5 \times 10^{17} \text{ cm}^{-3}$  and  $1 \times 10^{18} \text{ cm}^{-3}$  and maxima at 3.472 eV for  $[\text{Fe}] = 1 \times 10^{19} \text{ cm}^{-3}$  and  $2 \times 10^{20} \text{ cm}^{-3}$  (broadened) coincide with the values of free and bound excitons found for 400  $\mu\text{m}$  thick HVPE-grown GaN on sapphire.<sup>14</sup> Consequently, energy resulting from the bound exciton recombination is transferred to  $\text{Fe}^{3+}$  centers present at high Fe concentrations contributing to the  $\text{Fe}^{3+}$  luminescence. On the other hand, the recombination of the free exciton represents a competing process. A strong competition between the recombination via the free exciton and via the  $\text{Fe}^{3+}$  center was reported for ZnO.<sup>19</sup>

The spikes superimposed on the spectra of high Fe concentrations between 2.3 and 2.4 eV are attributed to internal transitions of Fe-related complexes, implying that despite careful choice of the detection window the defect luminescence (Fig. 6) was also detected. PLE spectra of the line at 1.268 eV yield an excitation band at the same position.<sup>28</sup> Considering the capture of free holes to be the most efficient excitation process of the  $\text{Fe}^{3+}$  luminescence, such defect luminescence is likely to represent competing recombination channels.

Finally, we observe an excitation band with peaks at 1.6 and 1.65 eV which clearly scales with the Fe concentration up to  $1 \times 10^{19} \text{ cm}^{-3}$  (see Fig. 12(a1)-(d1)). Its origin is still unclear. A possible interpretation is a generation of free holes via defects involved in the red luminescence (RL) occurring in GaN around 1.9 eV,<sup>43,44</sup> similar to the mechanism described above for the YL-defects.

#### IV. CONCLUSION

In this paper, the structural, optical and electronic properties of GaN doped with different concentrations of Fe were investigated. A good crystal quality and a strain-free incorporation of Fe on Ga site was proven by the EPR signal of  $\text{Fe}^{3+}$ , by the small FWHM of the ( ${}^4\text{T}_1(\text{G})\text{—}{}^6\text{A}_1(\text{S})$ ) luminescence and by the concentration-independent energy of the  $\text{E}_2(\text{high})$  phonon mode. Fe was observed in the charge states  $3+$  and  $2+$  by optical experiments. The respective electronic structures were established. For  $\text{Fe}^{3+}$ , besides the  ${}^6\text{A}_1(\text{S})$  ground state and the excited states  ${}^4\text{T}_1(\text{G})$ ,  ${}^4\text{T}_2(\text{G})$  and  ${}^4\text{E}(\text{G})$ , an effective-mass-like state consisting of a hole bound to  $\text{Fe}^{2+}$  ( $\text{Fe}^{2+}$ ,  $h_{\text{VB}}$ ) was established as the highest excited state of  $\text{Fe}^{3+}$ . With a binding energy of  $50\pm 10$  meV it represents a shallow transient acceptor state very similar to the same phenomenon in cubic III-V materials. While the fine structure of the  $\text{Fe}^{3+}({}^4\text{T}_1(\text{G}))$  state could be successfully established, we can only report the existence of a splitting for the  ${}^4\text{E}(\text{G})$  state ( $\sim 1.4$  meV) and the effective-mass-like state ( $\sim 8$  meV for both  $\text{Fe}^{2+}$  states). The fine structure of the latter reflects the splitting of the  $\text{Fe}^{2+}$  state involved in the bound state. For  $\text{Fe}^{2+}$ , we observed the internal ( ${}^5\text{E}\text{—}{}^5\text{T}_2$ ) transition at all studied Fe concentrations with the splitting of the  ${}^5\text{D}$  state amounting to 385 meV. Effective-mass-like complexes were observed involving both the  ${}^5\text{E}$  and the  ${}^5\text{T}_2$  state of  $\text{Fe}^{2+}$ , 2.812 eV and 3.127 eV above the  $\text{Fe}^{3+}$  ground state, respectively. The  $\text{Fe}^{3+/2+}$  charge transfer level was determined to be  $2.863\pm 0.005$  meV above the VB maximum. On the basis of this value, we conclude, that the internal reference rule does not hold

for GaN in conjunction with other III-V materials. No conclusion could be made regarding the heterojunction with AlN.

We found a strong coupling of internal  $\text{Fe}^{3+}$  transitions on  $\text{E}_2$  phonon modes and  $\text{A}_1$  and  $\text{E}$  LVMS. In contrast to cubic II-VI and III-V host materials, only a weak Jahn-Teller interaction effects the electronic states of both charge states. The reason is probably the reduced ligand field symmetry in  $c_{3v}$  configuration. At Fe concentrations from  $1\times 10^{19}$   $\text{cm}^{-3}$ , defect complexes involving Fe are formed which cause additional PL and EPR lines. The vibrational coupling is similar to that of isolated Fe centers. A very efficient excitation process for  $\text{Fe}^{3+}$  was proven to be the capture of free holes by  $\text{Fe}^{2+}$  centers. The holes are generated in a CT process from  $\text{Fe}^{3+}$  or in a two step process via the intrinsic shallow donor and the deep double donor involved in the YL. The results of our optical experiments suggest, that  $\text{Fe}^{2+}$  is present at all studied Fe concentrations, whereas  $\text{Fe}^{3+}$  only seems to exist at higher concentrations from  $1\times 10^{18}$   $\text{cm}^{-3}$ . Consequently, at these high concentrations, electron trapping by the Fe acceptor has lowered the Fermi level close to the  $\text{Fe}^{3+/2+}$  CT level, compensating intrinsic n-type conductivity. For higher Fe contents the Fermi level does not drop below the CT level but instead stays pinned to it, leading to a coexistence of  $\text{Fe}^{3+}$  and  $\text{Fe}^{2+}$ .

#### Acknowledgments

Financial support from the Australian Research Council is gratefully acknowledged.

\* corresponding author. E-mail address: [Malguth@physik.tu-berlin.de](mailto:Malguth@physik.tu-berlin.de); currently at Microstructural Analysis Unit, University of Technology, Sydney, Australia

† current address: WS Materials Technology, LLC, 15 Central St. Stamford, CT 06906, USA

<sup>1</sup> B. Monemar and O. Lagerstedt, *Journal of Applied Physics* **50**, 6480 (1979).

<sup>2</sup> R. P. Vaudo, X. Xu, A. Salant, J. Malcarne, and G. R. Brandes, *Physica status solidi (a)* **200**, 18 (2003).

<sup>3</sup> M. S. Shur and M. A. Khan, in *GaN and AlGaN Devices: Field Effect Transistors and Photodetectors*, edited by S. J. Pearton (Gordon and Breach, Amsterdam, 2000), pp. 47–92.

<sup>4</sup> T. Graf, S. T. B. Goennenwein, and M. S. Brandt, *physica status solidi (b)* **239**, 277 (2003).

<sup>5</sup> H. Ohno, *Science* **281**, 951 (1998).

<sup>6</sup> J. M. Langer and H. Heinrich, *Phys. Rev. Lett.* **55**, 1414 (1985).

<sup>7</sup> J. M. Langer, C. Delerue, M. Lannoo, and H. Heinrich, *Physical Review B* **38**, 7723 (1988).

<sup>8</sup> R. Heitz, P. Maxim, L. Eckey, P. Thurian, A. Hoffmann, I. Broser, K. Pressel, and B. K. Meyer, *Physical Review B* **55**, 4382 (1997).

<sup>9</sup> K. Maier, M. Kunzer, U. Kaufmann, J. Schneider, B. Monemar, I. Akasaki, and H. Amano, *Materials Science Forum* **143-147**, 93 (1994).

<sup>10</sup> J. Baur, K. Maier, M. Kunzer, U. Kaufmann, J. Schneider, H. Amano, I. Akasaki, T. Detchprohm, and K. Hiramatsu, *Applied Physics Letters* **64**, 857 (1994).

<sup>11</sup> R. Heitz, P. Thurian, I. Loa, L. Eckey, A. Hoffmann, I. Broser, K. Pressel, B. K. Meyer, and E. N. Mokhov, *Applied Physics Letters* **67**, 2822 (1995).

<sup>12</sup> L. Podlowski, R. Heitz, P. Thurian, A. Hoffmann, and I. Broser, *Journal of Luminescence* **48**, 252 (1994).

<sup>13</sup> E. Malguth, A. Hoffmann, and X. Xu, to be published (2006).

<sup>14</sup> B. K. Meyer, A. Hoffmann, and P. Thurian, in *Group III Nitride Semiconductor Compounds*, edited by B. Gil (Clarendon Press, Oxford, 1998), pp. 242–306.

<sup>15</sup> W. Gehlhoff, D. Azamat, U. Haboek, and A. Hoffmann, *Physica B: Condensed Matter Proceedings of the 23rd International Conference on Defects in Semiconductors* **376-377**, 486 (2006).

<sup>16</sup> A. Hoffmann, R. Heitz, and I. Broser, *Physical Review B* **41**, 5806 (1990).

<sup>17</sup> K. Pressel, G. Bohnert, G. Ruckert, A. Dornen, and

- K. Thonke, *Journal of Applied Physics* **71**, 5703 (1992).
- <sup>18</sup> K. Pressel, A. Dörnen, G. Rückert, and K. Thonke, *Phys. Rev. B* **47**, 16267 (1993).
- <sup>19</sup> R. Heitz, A. Hoffmann, and I. Broser, *Physical Review B* **45**, 8977 (1992).
- <sup>20</sup> J. Baur, K. Maier, M. Kunzer, U. Kaufmann, and J. Schneider, *Applied Physics Letters* **65**, 2211 (1994).
- <sup>21</sup> P. Thurian and A. Hoffmann, in *XIV Int. Symposium on Electron-Phonon Dynamics and Jahn-Teller-Effect, Erice, Italy, July 7-13, 1998*, edited by G. Bevilacqua, L. Martinelli, and N. Terzi (World Scientific, 1998), pp. 216–229.
- <sup>22</sup> K. Pressel, S. Nilsson, R. Heitz, A. Hoffmann, and B. K. Meyer, *Journal of Applied Physics* **79**, 3214 (1996).
- <sup>23</sup> H. Siegle, L. Eckey, A. Hoffmann, C. Thomsen, B. K. Meyer, D. Schikora, M. Hankeln, and K. Lischka, *Solid State Communications* **96**, 943 (1995).
- <sup>24</sup> V. Y. Davydov, Y. E. Kitaev, I. N. Goncharuk, A. N. Smirnov, J. Graul, O. Semchinova, D. Uffmann, M. B. Smirnov, A. P. Mirgorodsky, and R. A. Evarestov, *Phys. Rev. B* **58**, 12899 (1998).
- <sup>25</sup> P. Thurian, G. Kaczmarczyk, H. Siegle, R. Heitz, A. Hoffmann, I. Broser, B. K. Meyer, R. Hoffbauer, and U. Scherz, *Materials Science Forum* **196-201**, 1571 (1995).
- <sup>26</sup> C. Goebel, C. Schrepel, U. Scherz, P. Thurian, G. Kaczmarczyk, and A. Hoffmann, *Materials Science Forum* **258-263**, 1173 (1997).
- <sup>27</sup> F. Demangeot, J. Frandon, M. A. Renucci, O. Briot, B. Gil, and R. L. Aulombard, *Solid State Communications* **100**, 207 (1996).
- <sup>28</sup> P. Thurian, A. Hoffmann, L. Eckey, P. Maxim, R. Heitz, I. Broser, K. Pressel, B. K. Meyer, J. Schneider, J. Baur, et al., III-V Nitrides, *Materials Research Society Symposium Proceedings* pp. 707–712 (1997).
- <sup>29</sup> R. Heitz, P. Thurian, I. Loa, L. Eckey, A. Hoffmann, I. Broser, K. Pressel, B. K. Meyer, and E. N. Mokhov, *Physical Review B* **52**, 16508 (1995).
- <sup>30</sup> W. Gehlhoff, D. Azamat, and A. Hoffmann, *Physica status solidi (b)* **243**, 1687 (2006).
- <sup>31</sup> U. W. Pohl, H.-E. Gumlich, and W. Busse, *Physica Status Solidi (b)* **125**, 773 (1984).
- <sup>32</sup> L. Podlowski, R. Heitz, T. Wolf, A. Hoffmann, D. Bimberg, I. Broser, and W. Ulrici, in *Materials Science Forum* (1994), vol. 143-147, p. 311.
- <sup>33</sup> K. Pressel, G. Rückert, A. Dörnen, and K. Thonke, *Phys. Rev. B* **46**, 13171 (1992).
- <sup>34</sup> A. Juhl, A. Hoffmann, D. Bimberg, and H. J. Schulz, *Applied Physics Letters* **50**, 1292 (1987).
- <sup>35</sup> K. Thonke and K. Pressel, *Phys. Rev. B* **44**, 13418 (1991).
- <sup>36</sup> S. A. Ding, S. R. Barman, K. Horn, H. Yang, B. Yang, O. Brandt, and K. Ploog, *Applied Physics Letters* **70**, 2407 (1997).
- <sup>37</sup> B. K. Agrawal, S. Agrawal, and R. Srivastava, *Surface Science* **424**, 232 (1999).
- <sup>38</sup> G. Martin, A. Botchkarev, A. Rockett, and H. Morkoc, *Applied Physics Letters* **68**, 2541 (1996).
- <sup>39</sup> G. Rückert, K. Pressel, A. Dörnen, K. Thonke, and W. Ulrici, *Phys. Rev. B* **46**, 13207 (1992).
- <sup>40</sup> A. Hoffmann, L. Eckey, P. Maxim, J.-C. Holst, R. Heitz, D. M. Hofmann, D. Kovalev, G. Steude, D. Volm, B. K. Meyer, et al., *Solid State Electronics* **41**, 275 (1997).
- <sup>41</sup> D. M. Hofmann, D. Kovalev, G. Steude, B. K. Meyer, A. Hoffmann, L. Eckey, R. Heitz, T. Detchprom, H. Amano, and I. Akasaki, *Phys. Rev. B* **52**, 16702 (1995).
- <sup>42</sup> C. studies of the same set of GaN:Fe samples show that the yellow luminescence is significantly quenched with increasing Fe concentration. (????).
- <sup>43</sup> E. M. Goldys, M. Godlewski, T. Paskova, G. Pozina, and B. Monemar, *MRS Internet Journal of Nitride Semiconductor Research* **6** (2001).
- <sup>44</sup> I. C. spectra we observed the RL with a similar shape and position as in the present PLE studies. (????).